

## OH-initiated heterogeneous aging of highly oxidized organic aerosol

Sean H. Kessler<sup>1</sup>, Theodora Nah<sup>2,3</sup>, Kelly E. Daumit<sup>4</sup>, Jared D. Smith<sup>2</sup>, Stephen R. Leone<sup>3</sup>, Charles E. Kolb<sup>5</sup>, Douglas R. Worsnop<sup>5</sup>, Kevin R. Wilson<sup>2</sup>, Jesse H. Kroll<sup>1,4\*</sup>

<sup>1</sup> *Department of Chemical Engineering, Massachusetts Institute of Technology, Cambridge MA 02139*;

<sup>2</sup> *Chemical Sciences Division, Lawrence Berkeley National Laboratory, Berkeley CA 94720*;

<sup>3</sup> *Department of Chemistry, University of California, Berkeley, CA 94720*; <sup>4</sup> *Department of Civil and Environmental Engineering, Massachusetts Institute of Technology, Cambridge MA 02139*;

<sup>5</sup> *Center for Aerosol and Cloud Chemistry, Aerodyne Research Inc., Billerica MA 01821*

### Abstract

The oxidative evolution (“aging”) of organic species in the atmosphere is thought to have a major influence on the composition and properties of organic particulate matter, but remains poorly understood, particularly for the most oxidized fraction of the aerosol. Here we measure the kinetics and products of the heterogeneous oxidation of highly oxidized organic aerosol, with an aim of better constraining such atmospheric aging processes. Submicron particles composed of model oxidized organics—1,2,3,4-butanetetracarboxylic acid ( $C_8H_{10}O_8$ ), citric acid ( $C_6H_8O_7$ ), tartaric acid ( $C_4H_6O_6$ ), and Suwannee River fulvic acid—were oxidized by gas-phase OH in a flow reactor, and the masses and elemental composition of the particles were monitored as a function of OH exposure. In contrast to our previous studies of less-oxidized model systems (squalane, erythritol, and levoglucosan), particle mass did not decrease significantly with heterogeneous oxidation. Carbon content of the aerosol always decreased somewhat, but this mass loss was approximately balanced by an increase in oxygen content. The estimated reactive

uptake coefficients of the reactions range from 0.37 to 0.51 and indicate that such transformations occur at rates corresponding to 1-2 weeks in the atmosphere, suggesting their importance in the atmospheric lifecycle of organic particulate matter.

Keywords: organic aerosol, oxidative aging, heterogeneous oxidation, fulvic acid

## **Introduction.**

A major uncertainty in the prediction of the climate and health effects of fine atmospheric particulate matter is the extent to which organic particles may undergo physical and/or chemical changes over their atmospheric lifetimes<sup>1</sup>. Organic aerosol is, by definition, made up of reduced carbon, and so is expected to undergo oxidation in the atmosphere; however, the rates, products, and effects on aerosol properties of such oxidation reactions are not well constrained. Detailed studies of such effects have been impaired by the difficulty of reproducing the atmospheric formation of highly oxidized aerosol in the laboratory<sup>2-4</sup>. Additionally, the sheer chemical complexity of organic mixtures, which can consist of several thousands or millions of compounds<sup>5</sup>, further impedes exact chemical characterization of the organic aerosol.

In order to gain a better understanding key features of the chemistry of organic aerosol aging, we have recently carried out a number of studies on one class of aging reactions, the heterogeneous oxidation of organic particles by gas-phase hydroxyl radicals (OH). Such studies examined the oxidation of model single-component systems; these serve as rough surrogates for varying classifications and levels of oxidation of organic particles. Model systems examined previously include squalane ( $C_{30}H_{62}$ , a surrogate for primary, hydrocarbon-like organic aerosol)<sup>6,7</sup>, erythritol ( $C_4H_{10}O_4$ , a tracer for isoprene-derived secondary organic aerosol)<sup>8</sup>, and

levoglucosan ( $C_6H_{10}O_5$ , a key component of aerosol from biomass burning)<sup>8</sup>. This work indicated that as particles are progressively aged, the degree of oxidation of the particulate carbon increases. Moreover, volatilization processes become increasingly dominant at these higher levels of oxidation, leading to significant decreases in aerosol loading<sup>6,8</sup>.

Our previous work, and similar studies by other groups<sup>2,6-10</sup>, focused on the oxidation of relatively reduced organic aerosol, with average carbon oxidation states<sup>5</sup> of 0 or lower. Ambient measurements have shown that a large fraction of atmospheric organic aerosol is substantially more oxidized than this, with average carbon oxidation states as high as +1<sup>1,5</sup>. However, the reactivity (oxidation kinetics and products) of this oxidized organic aerosol is almost completely unconstrained at present; this limits our ability to accurately model the evolution and fate of atmospheric organic aerosol. The goal of this work is thus to study the oxidative aging chemistry of this already highly-oxidized aerosol in the laboratory. Because of the very low volatility of the constituent organics<sup>11-13</sup>, their fraction present in the gas phase is expected to be negligible, so that their oxidation must necessarily occur in the condensed phase. Therefore the aging mechanism probed in these experiments—heterogeneous oxidation by OH—is likely to be important in the atmospheric evolution of this class of organic aerosol.

## Methods

As in our previous studies of less-oxidized species, the aging kinetics and chemistry of the aerosol are probed by studying the heterogeneous oxidation of simpler, more chemically tractable model systems. The surrogate organics used in this study, chosen for their high oxidation states and low vapor pressures, are citric acid ( $C_6H_8O_7$ ; Aldrich, >99.5%), L-(+)-tartaric acid ( $C_4H_6O_6$ ; Aldrich, >99.5%), and 1,2,3,4-butanetetracarboxylic acid (BTA,  $C_8H_{10}O_8$ ;

Aldrich, 99%). Molecular structures of all three compounds are provided in Figure 1, along with average carbon oxidation state. Additionally, the aging of a more complex oxidized aerosol surrogate, Suwannee River fulvic acid (IHSS) is also examined. Measurements using the Aerosol Mass Spectrometer, described below, indicate that the average carbon oxidation state of unoxidized fulvic acid is ~0.6.

Heterogeneous oxidation experiments are carried out in the same flow reactor used in our prior studies; it has been described in detail previously<sup>6-8</sup> and is discussed only briefly here. The reactor is made up of type-219 quartz, with a length of 130 cm, inner diameter of 2.5 cm, and residence time of ~37 s. Carrier flow consists of 5% O<sub>2</sub> in N<sub>2</sub>, at 30% relative humidity. Particles are generated by atomizing and subsequently drying aqueous solutions of each of the starting compounds; the resulting particles, which have surface-weighted mean diameters of ~130-145 nm, are drawn into the flow reactor at loadings of ~500-650  $\mu\text{g m}^{-3}$ . These loadings are sufficiently high to ensure that at equilibrium over 99% of the starting compound is present in the condensed phase.

Ozone is produced by either a mercury pen-ray lamp or a commercial corona discharge ozone generator (OzoneLab Instruments). O<sub>3</sub> concentrations, which control the level of OH exposure within the reactor, are measured using an ozone monitor (2B Technologies Inc.). Within the flow reactor (temperature: 35 °C), ozone is photolyzed by UV light at 254 nm from two mercury lamps positioned immediately outside the quartz tube. O(<sup>1</sup>D) generated by ozone photolysis reacts with water vapor to form a pair of hydroxyl radicals (OH), which initiate oxidation of the particles. The water vapor concentration is maintained at a sufficiently high level to ensure that direct oxidation of organics by O(<sup>1</sup>D) is negligible, as determined previously<sup>7</sup>. Hexane (~100 ppb) added to the tube is monitored by GC-FID to quantify OH

concentration. This technique has been used to correctly predict rate constants in the reaction of OH with other selected gas-phase organics<sup>6,7</sup>; OH concentrations, which are changed by varying O<sub>3</sub>, range from  $\sim 1 \times 10^9$  to  $3 \times 10^{11}$  molecule cm<sup>-3</sup>. These concentrations correspond to atmospheric OH exposures of approximately one day to four weeks, assuming an average ambient OH concentration of  $3 \times 10^6$  molecule cm<sup>-3</sup>.

Particles exiting the flow reactor are sampled into a scanning mobility particle sizer (SMPS, TSI, Inc.), for the measurement of particle mobility diameters, and a high-resolution time-of-flight aerosol mass spectrometer (HR-ToF-AMS, Aerodyne Research, Inc.), for the measurement of particle composition and vacuum aerodynamic diameter. Particle mass is obtained from combined SMPS measurements and AMS particle-time-of-flight (PToF) data, by multiplying average particle volume (from the SMPS) by the effective particle density<sup>14</sup>. Although this method is strictly valid only for spherical particles, minor variations in particle shape will result in only small errors (<10%) in measured mass<sup>14</sup>. Measured effective densities do not vary significantly during the course of the experiments.

Particles of pure components do not change in composition or mass when the UV lights were turned on with no ozone added, verifying both that the parent organic compounds studied are not directly photolyzed, and that UV-generation of condensed-phase oxidants is negligible. Significant gas-phase oxidation of the compounds studied here is also highly unlikely, due to their strong partitioning into the particle phase and the short residence time in the flow reactor. Thus any changes to the mass or composition of the particles result from heterogeneous oxidation of particulate species by gas-phase OH radicals.

We characterize the chemical changes to the reacting systems in terms of changes to the overall elemental composition of organics in the condensed phase. In particular, the oxygen-to-

carbon ratio (O/C) and hydrogen-to-carbon ratio (H/C) are combined to estimate the overall degree of oxidation of the organic particles and the relative contributions of key functional groups. The method for calculating elemental ratios from high-resolution AMS data is described in detail by Aiken et al.<sup>15,16</sup>.

## Results and Discussion

Sample mass spectra of each of the model systems are presented in Figure 2. In all cases, the chemical composition of the aerosol was observed to change dramatically with OH exposure.

### *i. Oxidation Kinetics*

The rate of heterogeneous oxidation was quantified by measuring the decay of the parent compound, as estimated by a selected marker ion. The marker ion selected for each experiment was identified by spectral subtraction. The mass spectrum of the pure component in each system was scaled and subtracted from the average spectrum at every subsequent oxidant exposure level, so that the resulting residual spectrum contained no negative peaks beyond a specified tolerance (peaks contributing less than 0.1% of the total mass were ignored in order to avoid confounding effects of a small background signal). The ion that most frequently disappeared first in each system was chosen as the marker ion:  $\text{C}_4\text{H}_2\text{O}_3^+$  ( $m/z = 98$ ) for tartaric acid,  $\text{C}_4\text{H}_4\text{O}^+$  ( $m/z = 68$ ) for citric acid, and  $\text{C}_8\text{H}_8\text{O}_3^+$  ( $m/z = 152$ ) for BTA. Mass spectra of the three single-component systems and residual spectra from the highest level of oxidation are provided in Figure 2. In all cases, the residual spectra—which represent oxidation products—are dominated by low-mass fragment ions such as  $m/z$  44 ( $\text{CO}_2^+$ ) and so do not provide suitable marker ions for the study of subsequent generations of oxidation. The mass spectrum of unoxidized fulvic acid is also shown

in Figure 2; because it does not exhibit any sufficiently distinct marker ions, its kinetic behavior could not be determined.

The intensity of the selected marker ions are plotted in Figure 3 against OH exposure. Second-order rate constants for the reaction of the organic species with OH are estimated from an exponential fit using initial slopes, using only values corresponding to OH exposures below  $2 \times 10^{12}$  molecule s cm<sup>-3</sup>, since confounding secondary effects may slow the observed reaction rate at higher levels of oxidation<sup>2,8</sup>. The leveling-off observed for the marker ions at high OH exposures may be a result of a mass transfer limitation, which might prevent the oxidation of all of the parent species over the short timescale of the experiment (~37s). Rate constants, determined for each single-component aerosol type, are listed in Table 1.

From the second-order rate coefficients and other known parameters of the system, we also calculate the effective reactive uptake coefficient, defined as the ratio of the rate of reactive loss of the parent species to the OH collision rate with the particle surface<sup>7</sup>. The uptake coefficient is calculated from the rate constant according to

$$\gamma_{i,\text{OH}} = \frac{2D_0\rho_i N_A}{3\bar{c}_{\text{OH}} M_i} \chi(D_0) k_{i,\text{OH}} \quad (1)$$

where  $D_0$  is the surface-area-weighted mean particle diameter,  $\rho_i$  is the component density,  $M_i$  is the component molecular weight,  $N_A$  is Avogadro's number,  $c_{\text{OH}}$  is the mean speed of hydroxyl radicals, and  $\chi(D_0)$  is the diffusion correction factor<sup>17</sup>. Application of this correction accounts for a 15-30% increase in the calculated uptake coefficients. Uptake coefficients for the three single-component systems are listed in Table 1, with values ranging from 0.37 to 0.51. These values lie between the coefficient previously reported for squalane<sup>7</sup> and those of erythritol and

levoglucosan<sup>8</sup>, so we once again expect that heterogeneous oxidation will occur on atmospherically relevant timescales. Indeed, the lifetime against reaction with OH, estimated for particles with a diameter of 200 nm and an average OH concentration of  $3 \times 10^6$  molecule cm<sup>-3</sup>, ranges from 8 to 17 days (see Table 1), as compared with a depositional lifetime of ~10 days for similarly sized particles<sup>18</sup>.

## *ii. Elemental Analysis*

A van Krevelen plot in Figure 4 shows the oxidation trajectories of each of the four systems studied in terms of the hydrogen-to-carbon (H/C) and oxygen-to-carbon (O/C) ratios. In order to compare the results with similar studies of ambient organic aerosol<sup>19,20</sup>, we apply the method of Aiken et al.<sup>15,16</sup> with no additional correction factor. The measured H/C and O/C values of the pure compounds tend to be lower than their exact values; however, the overall trends observed in the trajectories remain unchanged, regardless of the correction factor used. The slope of the trajectory is indicative of the average chemical transformation of particulate organics<sup>19</sup>. For example, a slope of 0 corresponds to the addition of hydroxyl groups (oxygen addition with no net hydrogen loss), -2 corresponds to carbonyl addition, and steeper slopes denote the conversion of functional groups (e.g. hydroxyl to carbonyl, which involves a loss of hydrogen with no oxygen addition). On the other hand, if the oxidation reaction involves fragmentation—the cleavage of C-C bonds—and subsequent loss of carbon to the gas phase, then the resulting slope can take on a range of different values, depending on the chemical characteristics of the volatilized fragment. While previous studies have observed that measured ratios and trajectories of reduced and lightly oxidized organic aerosol follow a line with a slope of -1<sup>19</sup>, the data presented here have slopes ranging from -0.6 to -0.3 (Table 1). This tendency of

more highly oxidized systems to acquire oxygen with a smaller net loss of hydrogen is consistent with recent studies of the aging of oxidized organic aerosol<sup>20</sup>.

One possible reason for the shift in slopes may be that at higher oxidation levels, reactions leading only to oxygen addition, such as the formation of hydroxyl groups, are more strongly favored<sup>20</sup>. The volatility of oxidation products likely also plays an important role, since the elemental ratios are not those of the whole reaction system but rather only those in the particle phase. This effect can be illustrated by relating elemental ratios (position in van Krevelen space), carbon number, and vapor pressure. The contours in Figure 4 show the carbon number required for an organic compound to be present (at least 50%) in the particle phase under the conditions of the present experiments (i.e. where saturation vapor concentration equals aerosol loading<sup>21,22</sup>, ~500  $\mu\text{g m}^{-3}$ ). These contours were determined by relating each point in van Krevelen space to a functional group distribution, assuming only hydroxyl, carbonyl, and carboxylic acid functionalities and estimating vapor pressures for a given number of carbon atoms using the SIMPOL group additivity method<sup>23</sup>. The steep slope of these contours reflects the fact that hydroxyl groups affect vapor pressure more dramatically than do carbonyl groups<sup>23</sup>, so that there is not a perfect correspondence between oxidation state and volatility. Organic species with high O/C and H/C values (the upper-right of the van Krevelen plot) are the lowest in volatility and can therefore have a lower carbon number while remaining in the condensed phase. As a result, these species are more likely to remain in the particle phase even following fragmentation (C-C cleavage) reactions. Such reactions are most likely for highly oxidized species<sup>6</sup>, so this effect may explain the shallower slopes associated with the oxidation of highly oxidized species.

Figure 5 shows the particulate mass fraction remaining and the relative abundances of carbon and oxygen atoms in each of the systems studied, plotted against OH exposure. The exposure levels are adjusted to account for differences in particle size among experiments; the values presented are the estimated equivalent exposures for a particle with a surface-area-weighted mean diameter of 200 nm, using the relationship between rate coefficient and diameter presented in Equation (1). The slight increase in mass for the BTA and citric acid systems at the highest OH exposure level is attributed to fluctuation in the atomizer output, which causes the particle distribution to shift to larger diameters, rather than to a physical or chemical effect within the reactor. For each of the three pure-component systems, the loss of carbon by volatilization processes—principally fragmentation during oxidation—is offset by the addition of oxygen atoms, so that the total particle mass remains approximately constant. As a result, the primary effect of heterogeneous oxidation is to change particle composition (and therefore physicochemical properties), but not total mass. While there might be a mass transfer barrier that could prevent us from observing some eventual mass loss<sup>24</sup>, our previous studies on more reduced systems have demonstrated our capability for observing more significant mass changes on similar timescales<sup>8</sup>. Moreover, our observation that the particles do not experience a significant change in mass upon aging is consistent with results from recent field measurements, which find that particle O/C, but not mass, increases with photochemical age<sup>25-27</sup>.

## Conclusions

Summary plots of key changes to particles upon heterogeneous oxidation are provided in Figure 6 for all of the systems studied here, as well as those from our previous work (squalane, erythritol, and levoglucosan)<sup>6,8</sup>. Figure 6a shows the overall degree of oxidation of the condensed phase organics, as described by the average carbon oxidation state, approximated by the equation

$\overline{OS}_C \approx 2(O/C) - H/C^5$ . Regardless of the initial system chosen, there is invariably a marked increase in the level of oxidation upon exposure to OH. Furthermore, analysis of the atmospheric lifetimes of these compounds indicates that such chemical transformation by heterogeneous oxidation occurs on timescales commensurate with particle loss by deposition<sup>18</sup>. This is of particular significance for the lowest-volatility fraction of the oxidized organic aerosol, which is unlikely to be found in the gas phase and thus must undergo oxidation in the condensed phase—either by heterogeneous reaction with OH or via aqueous-phase chemistry<sup>28</sup>.

Additionally, Figure 6b shows the relative carbon content of each system as a function of OH exposure. Carbon loss serves as a useful proxy for volatilization of the particulate organic species; all systems exhibit some carbon loss, indicating that heterogeneous oxidation leads to the formation of oxidized species not only in the particle phase but in the gas phase as well. While the degree of carbon loss exhibits a good deal of variability from species to species, likely due to differences in carbon number and molecular structure, general trends with oxidation state are apparent. The least oxidized species (squalane, a saturated alkane) initially does not undergo any volatilization upon oxidation, due to the dominance of functionalization over fragmentation reactions<sup>5</sup>. As it gets more oxidized, however, further oxidation leads to significant loss of carbon (and total particle mass). This trend is also seen for the moderately oxidized species, erythritol and levoglucosan, which exhibit the most rapid volatilization. However, for the most oxidized species (the polycarboxylic acids examined in this work), carbon loss is restricted over the course of the experiment to no more than ~20%. This may be because fragmentation processes which otherwise contribute strongly to volatilization<sup>6</sup> either are less favored during oxidation or, more likely, produce fragments that are sufficiently low in volatility that they remain in the condensed phase. Furthermore, the loss of carbon for the most oxidized species is

typically offset by an equivalent increase in oxygen, so that the overall process approximately conserves particle mass. Atmospheric oxidation of the most oxidized organic aerosol is therefore unlikely to be a significant sink of aerosol mass, though it is still capable of transforming the chemical composition—and therefore key properties such as hygroscopicity<sup>1,29,30</sup> and refractive index<sup>30</sup>—of the particles over their atmospheric lifetimes.

## Acknowledgments

This work was supported by the National Science Foundation (Grants No. CHE-1012809 and AGS-1056225) and the Director, Office of Energy Research, Office of Basic Energy Sciences, Chemical Sciences Division of the U.S. Department of Energy under Contract No. DE-AC02-05CH11231. J.D.S. was supported by the Camille and Henry Dreyfus foundation postdoctoral program in environmental chemistry.

## References

- (1) Jimenez, J. L. et al. *Science* **2009**, *326*, 1525.
- (2) George, I. J.; Vlasenko, A.; Slowik, J. G.; Broekhuizen, K.; Abbatt, J. P. D. *Atmospheric Chemistry and Physics* **2007**, *7*, 4187–4201.
- (3) Lambe, A. et al. *Meas. Tech* **2011**, *4*, 445–461.
- (4) Lambe, A.; Onasch, T.; Massoli, P.; Croasdale, D.; Wright, J.; Ahern, A.; Williams, L.; Worsnop, D.; Brune, W.; Davidovits, P. *Atmos. Chem. Phys* **2011**, *11*, 8913–8928.
- (5) Kroll, J. H.; Donahue, N. M.; Jimenez, J. L.; Kessler, S. H.; Canagaratna, M. R.; Wilson, K. R.; Altieri, K. E.; Mazzoleni, L. R.; Wozniak, A. S.; Bluhm, H.; Mysak, E. R.; Smith, J. D.; Kolb, C. E.; Worsnop, D. R. *Nat Chem* **2011**, *3*, 133-139.

(6) Kroll, J. H.; Smith, J. D.; Che, D. L.; Kessler, S. H.; Worsnop, D. R.; Wilson, K. R. *Physical Chemistry Chemical Physics* **2009**, *11*, 8005–8014.

(7) Smith, J. D.; Kroll, J. H.; Cappa, C. D.; Che, D. L.; Liu, C. L.; Ahmed, M.; Leone, S. R.; Worsnop, D. R.; Wilson, K. R. *Atmospheric Chemistry and Physics Discussions* **2009**, *9*, 3945–3981.

(8) Kessler, S. H. Smith, J. D. Che, D. L. Worsnop, D. R. Wilson, K. R.; Kroll, J. H. *Environmental science & technology* **2010**, *44*, 7005-10.

(9) Rudich, Y. Donahue, N. M.; Mentel, T. F. *Annual Review of Physical Chemistry* **2007**, *58*, 321-352.

(10) George, I. J.; Abbatt, J. P. D. *Atmospheric Chemistry and Physics Discussions* **2010**, *10*, 3265-3300.

(11) Cappa, C.; Jimenez, J. *Atmospheric Chemistry and Physics* **2010**, *10*, 5409-5424.

(12) Huffman, J. et al. *Atmospheric Chemistry and Physics* **2009**, *9*, 7161-7182.

(13) Huffman, J. A. Docherty, K. S. Mohr, C. Cubison, M. J. Ulbrich, I. M. Ziemann, P. J. Onasch, T. B.; Jimenez, J. L. *Environmental Science & Technology* **2009**, *43*, 5351-5357.

(14) DeCarlo, P. Slowik, J. G. Worsnop, D. R. Davidovits, P.; Jimenez, J. L. *Aerosol Science and Technology* **2004**, *38*, 1185–1205.

(15) Aiken, A. C. DeCarlo, P. F.; Jimenez, J. L. *Anal. Chem* **2007**, *79*, 8350–8358.

(16) Aiken, A. C. et al. *Environ. Sci. Technol* **2008**, *42*, 4478–4485.

(17) Fuchs, N. A.; Sutugin, A. G. *Highly dispersed aerosols*; Halsted Press, New York, 1970.

(18) Kanakidou, M. et al. *Atmospheric Chemistry and Physics* **2005**, *5*, 1053–1123.

(19) Heald, C. L. Kroll, J. H. Jimenez, J. L. Docherty, K. S. DeCarlo, P. F. Aiken, A. C. Chen, Q. Martin, S. T. Farmer, D. K.; Artaxo, P. *Geophysical Research Letters* **2010**, *37*.

(20) Ng, N. Canagaratna, M. Jimenez, J. Chhabra, P. Seinfeld, J.; Worsnop, D. *Atmospheric Chemistry and Physics* **2011**, *11*, 6465–6474.

(21) Donahue, N. M. Robinson, A. L. Stanier, C. O.; Pandis, S. N. *Environmental Science & Technology* **2006**, *40*, 2635-2643.

(22) Odum, J. R. Hoffmann, T. Bowman, F. Collins, D. Flagan, R. C.; Seinfeld, J. H. *Environmental Science & Technology* **1996**, *30*, 2580-2585.

(23) Pankow, J. F.; Asher, W. E. *Atmos. Chem. Phys* **2008**, *8*, 2773–2796.

(24) Virtanen, A. et al. *Nature* **2010**, *467*, 824–827.

(25) Dunlea, E. et al. *Atmospheric Chemistry and Physics* **2009**, *9*, 7257–7287.

(26) Capes, G. Johnson, B.; McFiggans, G. *J. Geophys. Res* **2008**.

(27) DeCarlo, P. et al. *Atmospheric Chemistry & Physics* **2008**, *8*, 4027–4048.

(28) Ervens, B. Turpin, B.; Weber, R. *Atmos. Chem. Phys. Discuss* **2011**, *11*, 22301–22383.

(29) Massoli, P. et al. *Geophys. Res. Lett* **2010**, *37*, L24801.

(30) Cappa, C. D. Che, D. L. Kessler, S. H. Kroll, J. H.; Wilson, K. R. *Journal of Geophysical Research* **2011**, *116*, D15204.

## Tables

TABLE 1: Uptake Coefficients, Atmospheric Lifetime, and Van Krevelen Slope of Model Systems

|                                     | BTA                                | Citric Acid                     | Tartaric Acid                   | Fulvic Acid      |
|-------------------------------------|------------------------------------|---------------------------------|---------------------------------|------------------|
| $k^{(a)}$                           | $(7.6 \pm 2.4) \times 10^{-13(b)}$ | $(4.3 \pm 0.8) \times 10^{-13}$ | $(3.3 \pm 0.9) \times 10^{-13}$ | N.D.             |
| $\gamma_{i,\text{OH}}$              | $0.51 \pm 0.19$                    | $0.37 \pm 0.08$                 | $0.40 \pm 0.13$                 | N.D.             |
| Atmospheric Lifetime <sup>(c)</sup> | 8                                  | 13                              | 17                              | N.D.             |
| Van Krevelen Slope                  | $-0.31 \pm 0.02$                   | $-0.33 \pm 0.01$                | $-0.60 \pm 0.02$                | $-0.59 \pm 0.05$ |

<sup>(a)</sup>Units of rate coefficients are  $\text{cm}^3 \text{ molecule}^{-1} \text{ s}^{-1}$ . <sup>(b)</sup>All error bars reflect the 95% confidence intervals on the values provided. <sup>(c)</sup>Atmospheric lifetime is in days, assuming particles with a diameter of 200 nm at an average OH concentration of  $3 \times 10^6 \text{ molecule cm}^{-3}$ .

## Figure Captions

Figure 1. Molecular structures and average carbon oxidation state of the oxidized acids used in the single-component experiments in this study. Fulvic acid, which does not have a single defined structure, is therefore not pictured.

Figure 2. Aerosol mass spectra of reactants and products. (A,C,E,G) Mass spectra of unoxidized BTA, citric acid, tartaric acid, and fulvic acid, respectively. The spectra of the single-component systems (panels A, C, and E) contain several high-mass ion fragments, which are used to identify the relative amount of the starting compound left in the mixture at a given level of oxidation. (B,D,F) Product mass spectra of the oxidation of BTA, citric acid, and tartaric acid, respectively, determined by spectral subtraction of the unoxidized spectra from the most oxidized spectra. (H) Mass spectrum of oxidized fulvic acid at the highest OH exposure. Residual spectra, and the mass spectrum of unoxidized fulvic acid, are dominated by low-mass oxygenated ion fragments, consistent with ambient measurements of oxidized organic aerosol<sup>1</sup>.

Figure 3. Mass fraction remaining of key ions in the oxidation of the single-component systems.  $\text{C}_8\text{H}_8\text{O}_3^+$  ( $m/z = 152$ ) is used for BTA,  $\text{C}_4\text{H}_4\text{O}^+$  ( $m/z = 68$ ) for citric acid, and  $\text{C}_4\text{H}_2\text{O}_3^+$  ( $m/z = 98$ ) for tartaric acid. An initial-slope exponential fit, which only includes ions at exposures up to  $2 \times 10^{12}$  molecule s cm<sup>-3</sup>, is used to estimate the effective second-order rate coefficient for reaction with OH. The fitted trace is displayed over the data.

Figure 4. Van Krevelen diagram showing the elemental hydrogen-to-carbon (H/C) ratio vs. oxygen-to-carbon (O/C) at all points during the oxidation of the four systems in this study. The solid black line represents observations of ambient aerosol at moderate levels of oxidation<sup>19</sup>. The dashed black line represents measurements of ambient OOA at higher oxidation levels<sup>20</sup>. Red contours represent lines of constant volatility—the approximate number of carbon atoms a molecule must have at a given elemental composition in order to retain a saturation concentration of 500  $\mu\text{g m}^{-3}$ . As compounds become more oxidized, a shallower slope leads them more quickly to a region that allows a lower carbon content for the same volatility (or, conversely, lowers the volatility for a fixed number of carbon atoms).

Figure 5. Fractional mass contribution of carbon (red) and oxygen (blue), and total mass fraction remaining per particle (black) for each of the four systems over the course of oxidation. The x-axis in each plot is an effective OH exposure, adjusting to a mean particle diameter of 200 nm in each system. Total mass in each pure component system remains unchanged, as the loss of carbon is offset by an approximately equivalent increase in oxygen.

Figure 6. Summary of heterogeneous oxidation experiments. (A) Average carbon oxidation state as estimated from AMS elemental analysis<sup>5,15,16</sup> during the course of oxidation for squalane, erythritol, levoglucosan, and the systems introduced in this work. For consistency the same elemental analysis correction factors<sup>16</sup> are applied in all cases, and OH exposure is adjusted for a particle diameter of 200 nm (as in Figure 4). In general, there is an initial increase in oxidation state, at approximately the same rate, regardless of the system studied. (B) Estimated carbon loss, which serves as a measure of volatilization, for the same seven systems. Squalane, a reduced compound, undergoes moderate carbon loss. The moderately oxidized species, erythritol and levoglucosan, lose a much larger proportion of initial carbon to the gas phase, probably due to increased fragmentation reactions. On the other hand, the most oxidized species (the acids

examined in the present study) experience only mild volatilization, possibly because fragmentation products are so low in volatility that they remain in the condensed phase.

## Figures

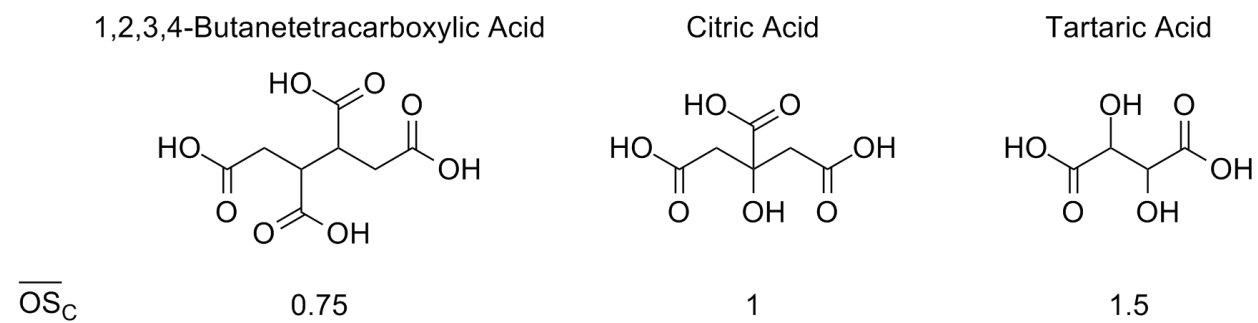


Figure 1

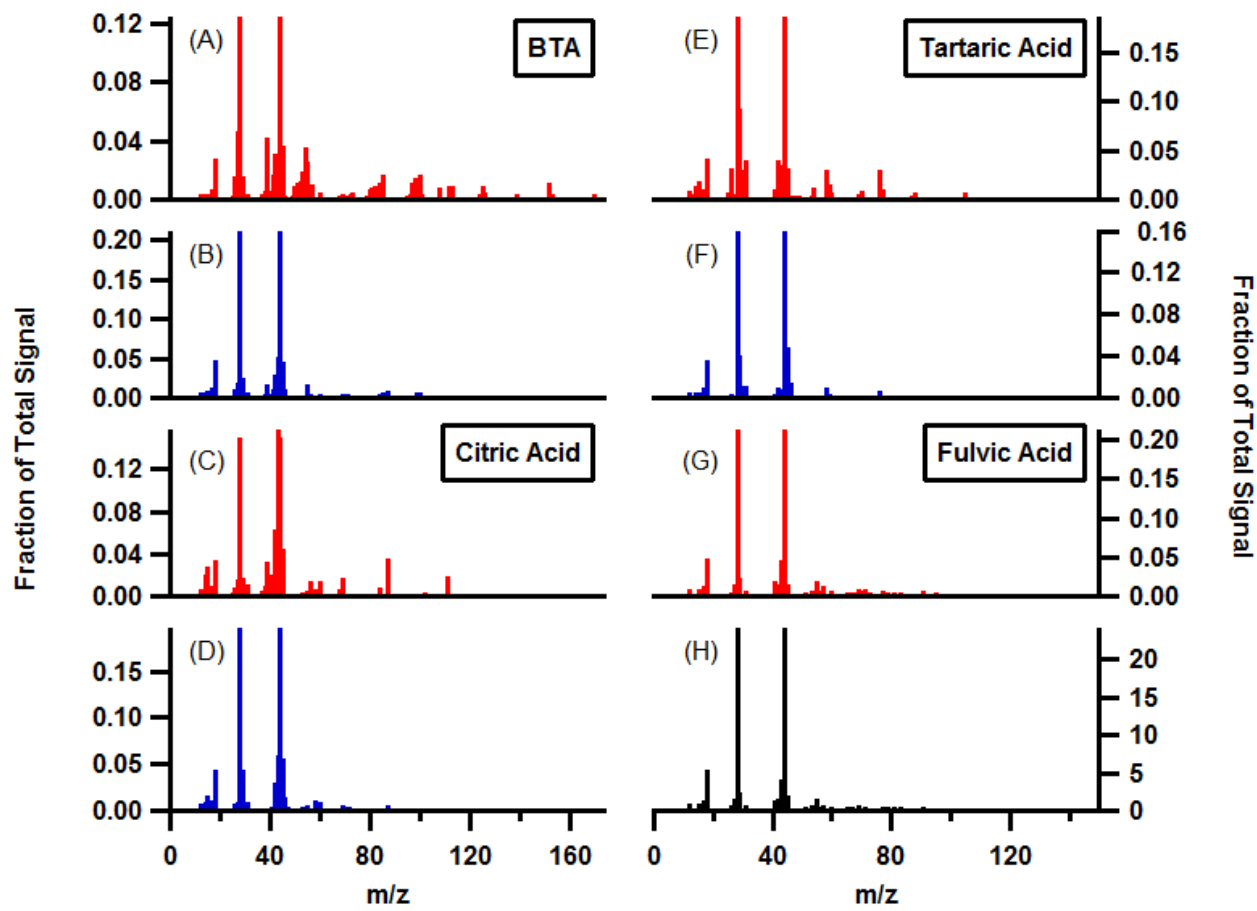


Figure 2

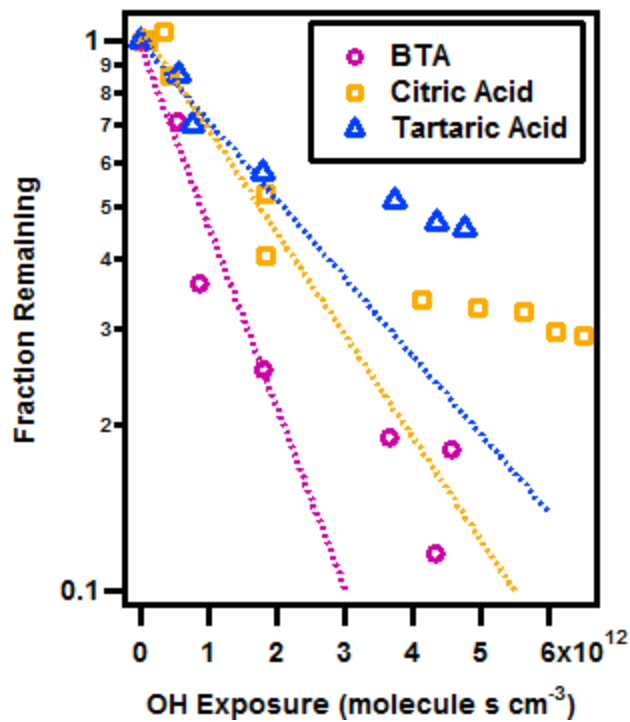


Figure 3

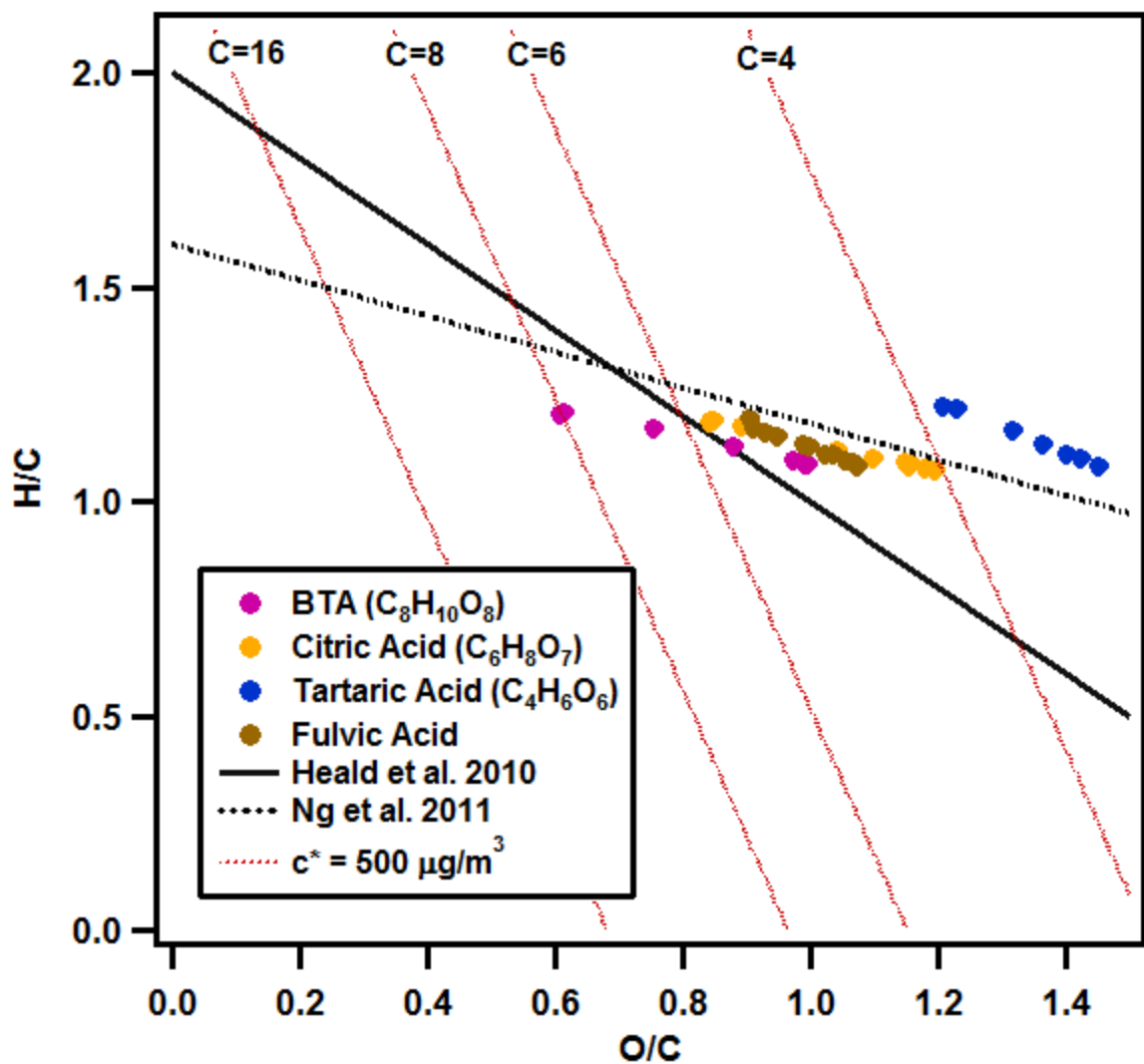


Figure 4

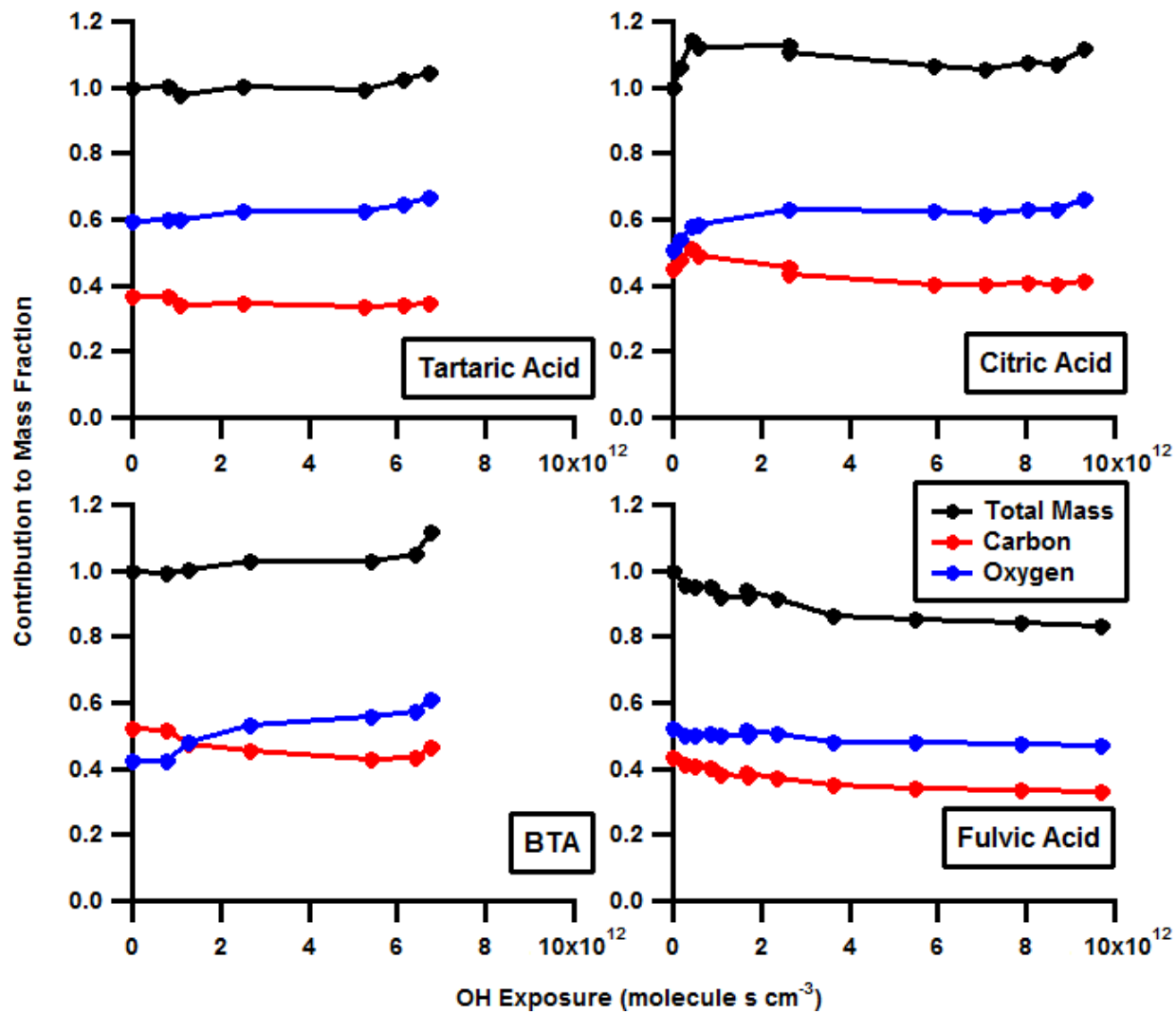


Figure 5

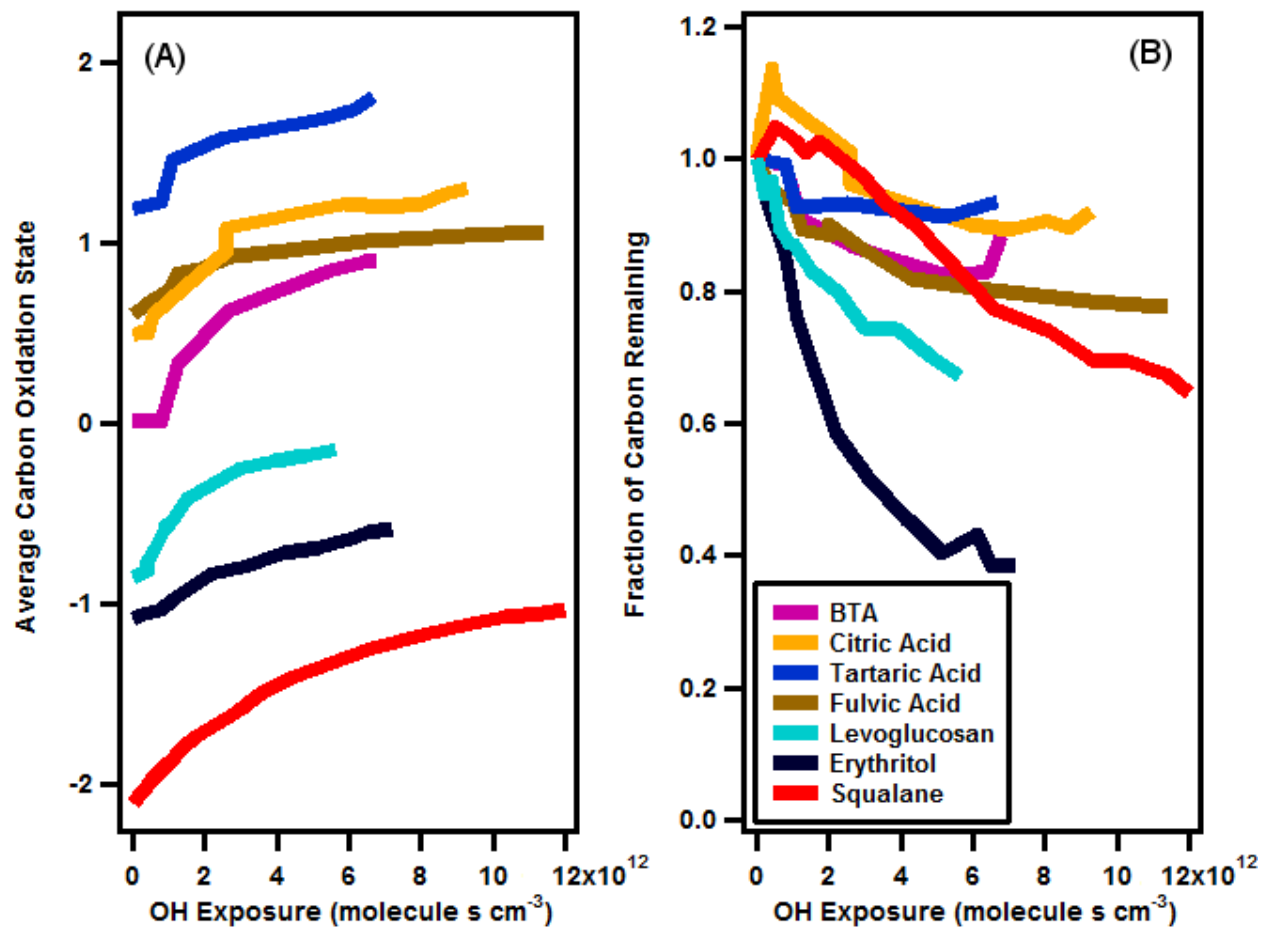


Figure 6

This document was prepared as an account of work sponsored by the United States Government. While this document is believed to contain correct information, neither the United States Government nor any agency thereof, nor the Regents of the University of California, nor any of their employees, makes any warranty, express or implied, or assumes any legal responsibility for the accuracy, completeness, or usefulness of any information, apparatus, product, or process disclosed, or represents that its use would not infringe privately owned rights. Reference herein to any specific commercial product, process, or service by its trade name, trademark, manufacturer, or otherwise, does not necessarily constitute or imply its endorsement, recommendation, or favoring by the United States Government or any agency thereof, or the Regents of the University of California. The views and opinions of authors expressed herein do not necessarily state or reflect those of the United States Government or any agency thereof or the Regents of the University of California.